Efficient seismic subsurface reconstruction by combining macro-velocity models and quantitative migrated images

H. Chauris[1], M. Benziane[1]

[1] Mines Paris

Summary

Least-squares reverse time migration (LSRTM) yields high-resolution subsurface reflectivity images by iteratively improving the fit between observed and synthetic reflected data. Approximate inverse strategies have been proposed to accelerate the convergence of LSRTM. These approximate inverses are typically formulated in the extended domain, meaning the data space and the model space share the same dimensionality. The resulting problem is solved using the linear conjugate gradient (LCG) method. Applications in synthetic settings demonstrate the effectiveness of approximate inverses, showing rapid convergence while yielding higher-resolution images compared to the standard approach.

Efficient seismic subsurface reconstruction by combining macro-velocity models and quantitative migrated images

Introduction

Iterative least-squares migration (LSM) derives images with higher resolution than those obtained with a single iteration of a standard adjoint approach (Nemeth et al., 1999). Under the Born approximation, we rely on a separation of scales: the velocity field is decomposed as the sum of a fixed macro-model and a velocity perturbation (image) to be updated. Theoretically, a perfect inverse operator implies that forward a modelling in the migrated image would exactly retrieve the original dataset. In practice, approximate inverses have been developed in recent years to approach this goal, particularly in the context of two-way subsurface-offset extended-domain linear modelling (ten Kroode, 2012; Hou and Symes, 2015, 2017, 2018; Chauris and Cocher, 2017; ten Kroode, 2023).

In the present study, we evaluate how such an approximate inverse can be introduced within a Linear Conjugate Gradient (LCG) minimisation process. We first review the expressions for the forward, adjoint, and inverse operators in the extended domain. We then present an iterative scheme and illustrate its effects on the Marmousi dataset, where only reflected waves are considered.

Forward, adjoint and approximate inverse

We remind the expressions for the forward, adjoint and approximate inverse in the subsurface extended domain (Chauris and Cocher, 2017). By *extended domain*, we mean that we consider two imaging points at positions $\mathbf{x}-\mathbf{h}$ and $\mathbf{x}+\mathbf{h}$, where $\mathbf{x}$ denotes the spatial position and $\mathbf{h}$ the subsurface offset. The z-component of this vector is usually set to zero, such that the dimensions of the data space $(\mathbf{s},\mathbf{r},\omega)$ and the image space $(\mathbf{x},\mathbf{h})$ match, where $\mathbf{s}$ and $\mathbf{r}$ correspond to the source and receiver positions, respectively, ω is the angular frequency.

In a given macro-model v_0 and a given velocity perturbation δv, the forward modelling in the extended domain reads

$$\delta d(\mathbf{s},\mathbf{r},\omega) = F\delta v = (i\omega)^2\Omega(\omega)\iint \mathrm{d}\mathbf{x}\,\mathrm{d}\mathbf{h}\, G_0(\mathbf{s},\mathbf{x}-\mathbf{h},\omega)\frac{2\delta v(\mathbf{x},\mathbf{h})}{v_0^3}G_0(\mathbf{r},\mathbf{x}+\mathbf{h},\omega). \tag{1}$$

In the standard Born approximation ($\mathbf{h}=0$), scattering is assumed to be a purely local process occurring at a single image point $\mathbf{x}$. In the extended domain formulation (Equation 1), this scattering process becomes non-local: the first Green's function $G_0(\mathbf{s},\mathbf{x}-\mathbf{h},\omega)$ propagates the source wavefield from the source $\mathbf{s}$ to the image point $\mathbf{x}-\mathbf{h}$. The energy is then scattered by the extended perturbation $\delta v(\mathbf{x},\mathbf{h})$ and emerges at a the image point $\mathbf{x}+\mathbf{h}$ from which the second Green's function $G_0(\mathbf{r},\mathbf{x}+\mathbf{h},\omega)$ propagates the wavefield to the receiver $\mathbf{r}$. $\Omega(\omega)$ denotes the source wavelet.

The adjoint of the forward modelling operator F is the key element in LCG to determine the optimal velocity perturbation. It involves back-propagating the data residuals, which reads

$$\xi_{\mathrm{adj}}(\mathbf{x},\mathbf{h}) = F^t\delta d = \frac{2}{v_0^3}\iiint \mathrm{d}\omega\,\mathrm{d}\mathbf{s}\,\mathrm{d}\mathbf{r}\,(i\omega)^2\Omega^*(\omega)G_0^*(\mathbf{s},\mathbf{x}-\mathbf{h},\omega)\delta d(\mathbf{s},\mathbf{r},\omega)G_0^*(\mathbf{r},\mathbf{x}+\mathbf{h},\omega). \tag{2}$$

Here, the complex conjugate (*) applied to the Green's functions and the seismic wavelet accounts for the time-reversed propagation, while the integration variables differ. Following Chauris and Cocher (2017), we propose an approximate inverse defined as a weighted adjoint denoted $F^\dagger$, such that $\delta d \simeq FF^\dagger\delta d$, reading

$$\xi_{\mathrm{inv}}(\mathbf{x},\mathbf{h}) = F^\dagger\delta d = -16v_0\partial_z\iiint \mathrm{d}\omega\,\mathrm{d}\mathbf{s}\,\mathrm{d}\mathbf{r}\,\frac{1}{i\omega}\Omega^\dagger(\omega)\partial_{s_z}G_0^*(\mathbf{s},\mathbf{x}-\mathbf{h},\omega)\delta d(\mathbf{s},\mathbf{r},\omega)\partial_{r_z}G_0^*(\mathbf{r},\mathbf{x}+\mathbf{h},\omega). \tag{3}$$

Here are the main differences between the adjoint and approximate inverse expressions: (1) the conjugate of the source wavelet is replaced by the inverse $\Omega^\dagger(\omega) = \Omega^*/(|\Omega|^2+\varepsilon)$, with ε acting as a regularisation term. (2) Vertical derivatives ∂_{s_z}, ∂_{r_z} and ∂_z are applied in front of the Green's functions and after the imaging condition. They act as a multiplication by the cosine of the emerging angles at the surface and by the cosine of the angle at the imaging point (see below). (3) Finally, different terms ($-16v_0$ and $1/i\omega$) are introduced to get the correct amplitudes and phase terms.

Formally, the approximate inverse acts as a source deconvolution and compensates for geometrical amplitude spreading and uneven illumination (ten Kroode, 2012). As an intermediate step, we rely on the high-frequency approximation (geometrical optics) for the expression of the Green's function $G(\mathbf{s},\mathbf{x},\omega) \simeq K(\omega)A(\mathbf{s},\mathbf{x})e^{i\omega\tau(\mathbf{s},\mathbf{x})}$, where A and τ are smoothly varying amplitude and travel time terms, and K is a function only depending on ω. In 2d, $K(\omega) = 1/\sqrt{i\omega}$. The application of the vertical derivative ∂_z to the Green's function acts as a multiplication by the cosine of the angle at the image point according to

$$\partial_z G = K(\omega)\left(\partial_z A + i\omega\partial_z\tau A\right)e^{i\omega\tau(\mathbf{s},\mathbf{x})} \simeq K(\omega)i\omega\partial_z\tau A e^{i\omega\tau(\mathbf{s},\mathbf{x})} = i\omega\partial_z\tau G(\mathbf{s},\mathbf{x},\omega) = i\omega\frac{\cos\theta}{v_0(\mathbf{x})}G(\mathbf{s},\mathbf{x},\omega). \tag{4}$$

For this simplification, we assume the high-frequency limit ($\omega \gg 1$). We then recognise the expression of the Green's function multiplied by $i\omega\partial_z\tau$. Intermediate steps for the derivation of Equation 3 yield $\cos\theta$ terms, which are replaced by spatial derivatives and additional adjustments in $i\omega$ and v_0 (Hou and Symes, 2015; Chauris and Cocher, 2017). The final expression in Equation 3 no longer contains asymptotic terms.

Iterative schemes

Starting with $\xi_{\text{adj}} = 0$ and $\xi_{\text{inv}} = 0$, we propose two iterative approaches for minimising the least-squares objective function $J[\xi] = {}^1\!/\!_2\left\|F\xi - \delta d_{\text{obs}}\right\|^2$.

Approach A – standard Linear Conjugate Gradient. The standard approach reads

$$\begin{aligned} r_n &= F^t(F\xi_n - \delta d_{\text{obs}}), && (5)\\ p_n &= -r_n + \beta_n p_{n-1}, && (6)\\ \xi_{n+1} &= \xi_n + \alpha_n p_n, && (7) \end{aligned}$$

where β_n is a coefficient to ensure conjugate directions, r_n the standard gradient and p_n the descent directions.

Approach B – preconditioned Linear Conjugate Gradient. With the use of the approximate inverse, we propose a modified approach reading

$$\begin{aligned} r_n &= F^\dagger(F\xi_n - \delta d_{\text{obs}}), && (8)\\ \xi_{n+1} &= \xi_n - r_n, && (9) \end{aligned}$$

where we do not consider the conjugate directions and where the step length $\alpha_n = 1$: it means that per iteration, one needs to apply F and $F^\dagger$ (same cost as for F^t), whereas in the classical preconditined approach (not shown here), there is an overhead for applying $F^\dagger$.

Results

We evaluate the approach on the 2d Marmousi model, where only reflected waves are considered. Recall that v_0 is fixed (Figure 1). The main characteristics are the following: $f_{\max} = 25$ Hz. $dx = dz = 12.5$ m and $dt = 1.63$ ms, with sources and receivers at the surface and a maximum surface (with negative and positive offset) of 1560 m.

After 1 and 10 iterations with Approach A (standard LCG), the structures are revealed (Figure 2). Hereafter, we display $v = v_0 + \delta v$, noting that only δv is updated and δv is obtained by stacking ξ over all subsurface offset (Dafni and Symes, 2018).

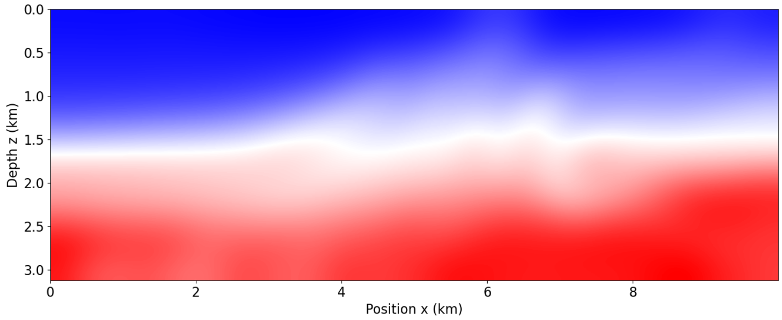

Figure 1: Initial velocity field

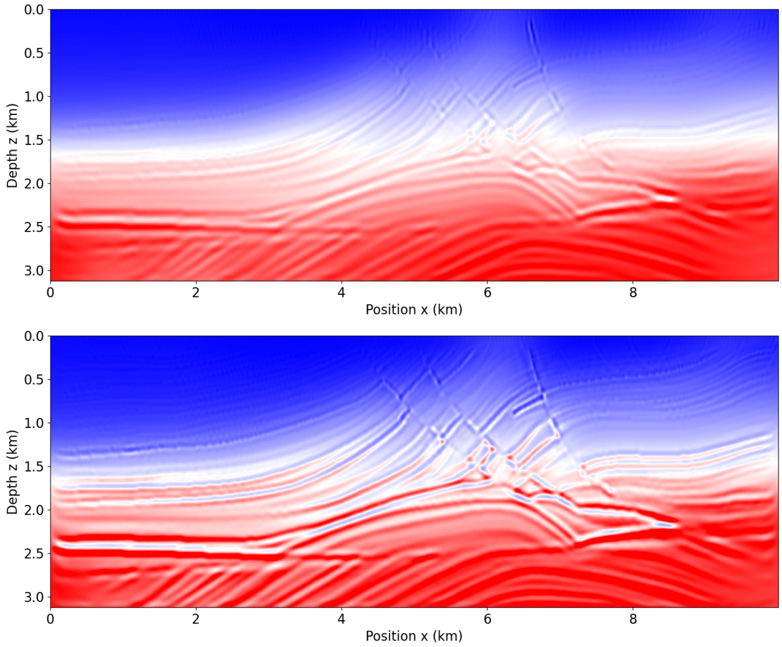

Figure 2: Velocity field after 1 (top) and 10 (bottom) adjoint iterations (approach A).

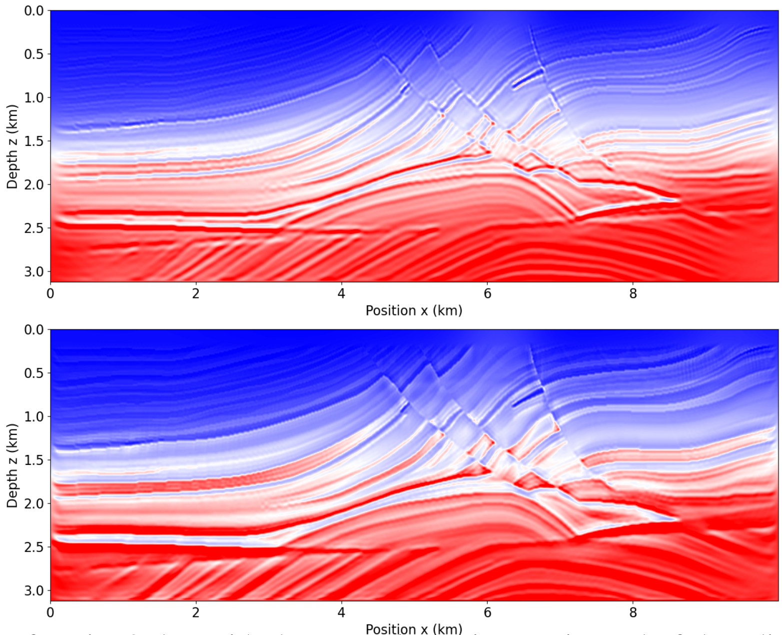

Figure 3: Same as for Fig. 2, but with the approximate inverse instead of the adjoint approach (approach B).

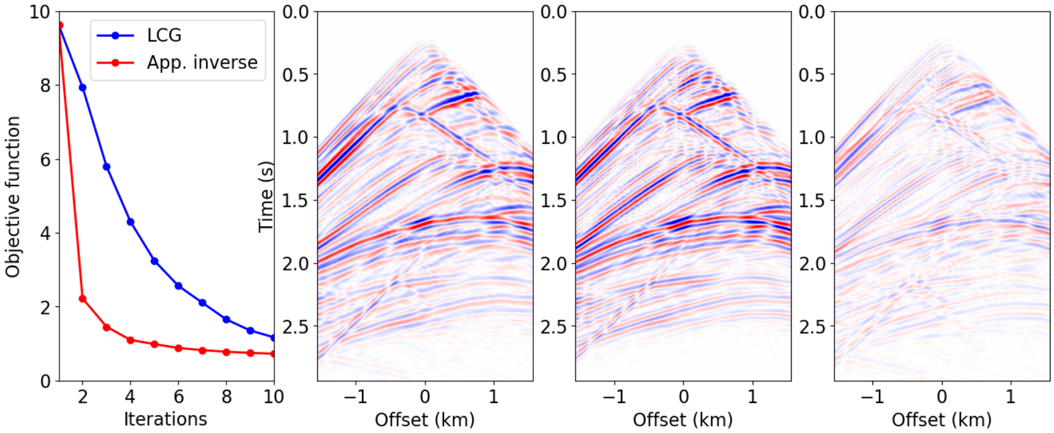

Figure 4: From left to right: (1) shape of the least-squares data misfit objective functions, for approaches A (blue) and B (red), (2) observed shot gather (only the reflected waves), (3) reconstructed shot gather after 1 iteration with the preconditioned approach, (4) differences between the observed and constructed data.

After 1 iteration with Approach B, the quality of the focusing is even better than after 10 iterations in Approach A (Figure 3, top). More iterations better reconstruct the layers between the main interfaces (Figure 3, bottom). The objective function for approach B decreases faster than the one for approach A (Figure 4, left). Here, iteration corresponds to n or equivalently to one application of F and F^t or $F^\dagger$. Finally, we display the original data, the inverted data after one iteration (Approach B) and the data residuals (Figure 4, right), confirming the validity of the approximate inverse.

It is also possible to add regularisation terms in the iterative process (approaches A and B), in particular in the case of sparse acquisition geometries (Farshad and Chauris, 2021). $\xi(\mathbf{x},\mathbf{h})$ also offers the possibility to estimate the quality of the focusing and updating the macro-model (Chauris and Cocher, 2017).

Conclusions

In the context of iterative least-squares migration, we have proposed a very simple iterative scheme in which the approximate inverse applied to the data residuals is used to update the image, for the same cost per iteration as the standard LCG. The approach has been validated on a 2d complex synthetic data set. The next steps require to consider applications to field data sets as well as the extension to 3d.

Acknowledgements

The authors would like to thank the Carnot M.I.N.E.S for partly funding the project.

References

Chauris, H. and Cocher, E. [2017] From migration to inversion velocity analysis. *Geophysics*, **82**(3), S207–S223.

Dafni, R. and Symes, W.W. [2018] Asymptotic inversion of the variable density acoustic model. In: *Expanded Abstracts*. Society of Exploration Geophysicists, 570–574.

Farshad, M. and Chauris, H. [2021] Sparsity–promoting multi–parameter pseudoinverse Born inversion in acoustic media. *Geophysics*, **86**(3), S205–S220.

Hou, J. and Symes, W.W. [2015] An approximate inverse to the extended Born modeling operator. *Geophysics*, **80**(6), R331–R349.

Hou, J. and Symes, W.W. [2017] An alternative formula for approximate extended Born inversion. *Geophysics*, **82**(1), S1–S8.

Hou, J. and Symes, W.W. [2018] Inversion velocity analysis in the subsurface–offset domain. *Geophysics*, **83**(2), R189–R200.

ten Kroode, A.P.E. [2012] A wave–equation–based Kirchhoff operator. *Inverse Problems*, **28**, 115013.

ten Kroode, A.P.E. [2023] An omnidirectional seismic imagine extension. *Inverse Problems*, **39**, 035003.

Nemeth, T., Wu, C. and Schuster, G.T. [1999] Least–squares migration of incomplete reflection data. *Geophysics*, **61**(1), 208–221.